

# Synchronization of fluctuating chaotic networks

Manuel Jimenez Martin,<sup>1</sup> Javier Rodríguez-Laguna,<sup>1</sup> Javier de la Rubia,<sup>1</sup> and Elka Korutcheva<sup>1,2</sup>

<sup>1</sup>*Departamento de Física Fundamental, UNED, Spain\**

<sup>2</sup>*G. Nadjakov Inst. Solid State Physics, Bulgarian Academy of Sciences, 1784, Sofia, Bulgaria*

(Dated: December 9, 2024)

We consider the synchronization of identical chaotic units connected through time-delayed interactions when the interaction network fluctuates. A random alternation of network structures can, in fact, enhance the synchronizability. We focus on fluctuating small-world networks of Bernoulli and Logistic units with a fixed chiral backbone, performing a previous study of their static behavior. Synchronized states appear to be maximally stable when fluctuations are much faster than the time-delay, even when the instantaneous state of the network does not allow synchronization. On the other hand, the enhancing effect disappears for very slow fluctuations. For fluctuation time scales of the order of the time-delay, a desynchronizing resonance is reported. Oscillations are observed in the variance between the states of the units, with periods related to the time-delay and its square.

Keywords:

## I. INTRODUCTION

The cooperative behavior of chaotic systems in interaction can lead to the emergence of partial and local synchronization [1]. An interesting problem is the stability of the synchronized state, which is ruled by the topology of the interaction network through the spectrum of its adjacency matrix [2, 3]. In certain settings, the coupling terms carry a time-delay due to the finite velocity of transmission of information. Yet, even for infinitely large time-delay the units can achieve zero-lag synchronization [4]. The paradigmatic time-delayed coupled systems capable of chaos synchronization are semiconductor lasers [5, 6], but there are interesting applications on neuroscience [7, 8] and secure communication [9, 10].

Theoretical studies are limited to specially simple chaotic systems, such as Bernoulli maps under single [11, 12] or multiple [13] time-delays, for which the conditions for synchronization can be obtained analytically. These studies generally perform a stability analysis of the synchronized state on a fixed interaction network. It is then logical to inquire about what happens when we introduce disorder on the topology. A general formalism has also been developed for ensembles of static random interaction networks [14]. The synchronization stability problem becomes more complex when one considers random and time-varying topologies [15]. Recently, there has been a number of studies on synchronization on time-varying contact networks, where the topology changes due to the random motion of the agents and the couplings are instantaneous. Most of them consider diffusive coupling of moving oscillators [16, 17], but also chaotic units [18, 19]. In this paper we study the synchronization properties of chaotic maps interacting on random small-world directed networks whose topology fluctuates in time and whose links bear a large time-delay. There has been a

very recent work concerning the case of coupled chaotic maps interacting with small time-delays comparable to the time scale of network switching [20]. Our work builds on the previous studies by exploring synchronization stability on the full range of possible scalings between the time-delay and the network switching time scale.

Let us consider an interaction network of coupled Bernoulli maps with a single time-delay,  $T_d$ , and let us denote the characteristic time-scale associated to the network fluctuations as  $T_n$ . If  $T_n \gg T_d$ , i.e., the slow network regime, the dynamics always have enough time to adapt to the current network. Therefore, if the network acquires a desynchronizing configuration, it will lose synchronization. Re-synchronization, although possible in principle, is unlikely. Thus, we may regard the long term dynamics as desynchronized whenever the probability of reaching a non-synchronizing network is finite. The case where  $T_n$  is comparable to  $T_d$  or smaller is more involved. Indeed, the system will spend time both in synchronizing and de-synchronizing networks. When the network reaches a de-synchronizing configuration, it will start to escape the synchronization manifold. But, if  $T_n$  is not large enough, there is a probability of returning to a synchronizing configuration before a certain *irreversibility line* is crossed. Thus, the system may stay synchronized. Indeed, our results will prove stronger: when  $T_n \ll T_d$ , in the fast fluctuations regime, synchronization becomes significantly more stable. This is in qualitative agreement with the fast switching approximation [21], which states that synchronization is possible for fast fluctuating networks and diffusive coupling if the time averaged graph laplacian synchronizes. Notice that the network fluctuations considered in this work are *not* adaptive, i.e., the network evolution is not linked to the state in any way.

This paper is organized as follows. Section II defines our time-delayed dynamical system, and reviews the basic framework for its study. In section III we study in detail the synchronizability in the case of (static) small-world networks. Then, we define our fluctuating networks, the observables to be employed, and discuss the

---

\*Electronic address: manuel.jimenez@fisfun.uned.es

numerical results in detail in IV. The last section is devoted to the conclusions and further work.

## II. SYNCHRONIZATION OF DELAYED CHAOTIC NETWORKS

Let us consider  $N$  classical units, characterized by a single degree of freedom  $u_i(t)$ ,  $i \in \{1, \dots, N\}$  and time  $t \in \mathbb{N}$ , whose evolution is given by:

$$u_i(t+1) = (1-\epsilon)f(u_i(t)) + \epsilon \sum_j G_{ij}(t)f(u_j(t-T_d)), \quad (1)$$

where  $\epsilon \in [0, 1]$  is a real parameter which measures the relevance of the interaction,  $T_d$  is a certain delay time,  $f : [0, 1] \mapsto [0, 1]$  is a chaotic map, such as the Bernoulli map,

$$f(x) = ax \mod 1, \quad (2)$$

with  $a \in \mathbb{R}^+$ , or the Logistic map,

$$f(x) = rx(1-x), \quad (3)$$

with  $r \in \mathbb{R}^+$ . The couplings form a generally directed network with adjacency matrix entries  $G_{ij}$  ( $\neq G_{ji}$ ). The couplings are subject to a unit row-sum condition (also known as stochasticity condition),

$$\sum_j G_{ij}(t) = 1, \quad (4)$$

for all  $i$  and all times  $t$ . This condition is sufficient to ensure the *existence* of a synchronized dynamical state: if at a certain moment all units have *exactly* the same value,  $u_i(t_0) = s$ , then they will stay synchronized for all future times. Nonetheless, this does not inform us about the stability of such synchronized state. The next paragraphs are devoted to the characterization of the synchronization level and its stability.

As a measure of the synchronization level, assuming for simplicity only zero-lag synchronization, we have chosen the logarithm of the spatial variance of the state. Let us explain in detail the meaning of this observable. Consider the spatial average of the unit states for a given time as

$$\mu_u(t) \equiv \frac{1}{N} \sum_{i=1}^N u_i(t), \quad (5)$$

and the corresponding spatial variance as

$$\sigma_u^2 \equiv \frac{1}{N} \sum_{i=1}^N (u_i - \mu_u)^2. \quad (6)$$

Then, the *synchronization level* is defined as

$$\mathcal{S} \equiv -\ln(\sigma_u^2). \quad (7)$$

A perfectly synchronized state would have  $\mathcal{S} \rightarrow +\infty$ , but in practice this value is bounded by the machine precision. In our calculations, using double precision floating point numbers, this value corresponds approximately to  $\mathcal{S} \sim 70$ , which implies a variance of order  $\sigma_u^2 \sim \exp(-70) \sim 10^{-30}$ . On the other extreme, a desynchronized state has a variance  $\sigma_u^2$  of order  $1/N$ , thus  $\mathcal{S} \sim \ln(N)$  takes a much lower value. In our experiments, with  $N$  of order 10 to 100, the minimal value of  $\mathcal{S}$  is around  $\ln(100) \sim 5$ .

The initial condition for our numerical experiments will always be nearly-synchronized state, in which all

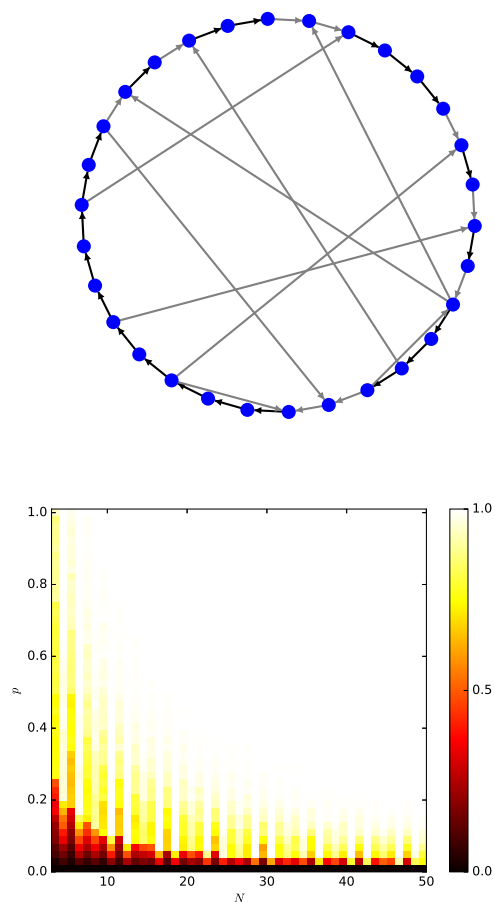


Figure 1: Top: Illustrating the directed networks used in our dynamical systems. In the example, a  $N = 30$  network with a clockwise rotating backbone and  $p = 0.3$ , so the number of shortcuts is  $N_s = 9$ . The strength of each link is denoted by its color: black is 1 and gray is  $1/2$ . Notice that the sum of input links on any node is always 1, as imposed in Eq. (4). Bottom: Average fraction of the networks having  $GCD = 1$  in the  $N \times p$  space. For high enough number of units and shortcuts the probability of  $GCD > 1$  is negligible.

units evolve in unison for  $T_d$  time steps, after which a random perturbation,  $\xi = A \cdot \mathbf{r}$ , of amplitude  $A = 10^{-10}$  acts on all of them, where  $\mathbf{r}$  is a vector of random numbers drawn uniformly from  $[0, 1]$ . Thus, the initial synchronization level is always around 50, instead of the machine precision value of 70. We will denote by  $\langle \cdot \rangle$  the *realization average* over such initial conditions. Our most relevant observable, therefore, will be  $\langle \mathcal{S}(t) \rangle$ .

We define a *synchronization Lyapunov exponent* (SLE), in similarity to the master stability function [2], as the average linear rate at which the synchronization level increases or decreases with time:

$$\langle \mathcal{S}(t) \rangle \sim \mathcal{S}_0 - \lambda t. \quad (8)$$

If  $\lambda < 0$  the synchronized state is stable, and unstable if  $\lambda > 0$ .

For directed chaotic networks with a single time-delay, the stability of the synchronized state is related to the spectrum of the adjacency matrix  $G$ . Let  $\{\gamma_i\}_{i=1}^N$  be the eigenvalues of  $G$ . Gerschgorin circle theorem [22] can be applied, and we can show that  $|\gamma_i| \leq 1$ . Indeed, there is always an eigenvalue  $\gamma_1 = 1$ . Let us sort them in descending order of their modulus,  $|\gamma_1| \geq |\gamma_2| \geq \dots \geq |\gamma_N|$ . Then, we define the *spectral gap* as  $\Delta = |\gamma_1| - |\gamma_2| = 1 - |\gamma_2|$ .

For the Bernoulli map, Eq. (2), there is a condition for synchronization [23]:

$$\epsilon > \frac{a-1}{a\Delta}. \quad (9)$$

In order to prove this inequality we require that the stretch factor of the map  $|f'(x)|$  be uniform in  $[0, 1]$ , which is fulfilled for the Bernoulli map.

### III. SYNCHRONIZATION OF SMALL-WORLD STATIC NETWORKS

Let us discuss the effects on synchronization of the topology of the interaction network, codified into its adjacency matrix  $G_{ij}$ . It has been shown previously that small world networks facilitate synchronization [24]. Here, we will consider a family of Newman-Watts networks [25], similar to the standard small-world [26] but keeping the outside ring fixed, so that it is guaranteed that the network is always connected. We will refer generically to these networks as small world (SW).

Consider a chiral 1D chain of  $N$  sites, where the only non-zero entries have the form  $G_{i,i+1}$ , with periodic boundary conditions. Let  $p \in \mathbb{R}^+$ , then we add to the chiral backbone a number  $\langle pN \rangle$  of directed *shortcuts*, connecting random sites. An example of such a SW network, with  $N = 30$  and  $p = 0.3$  is shown in Fig. 1 (top) for illustration.

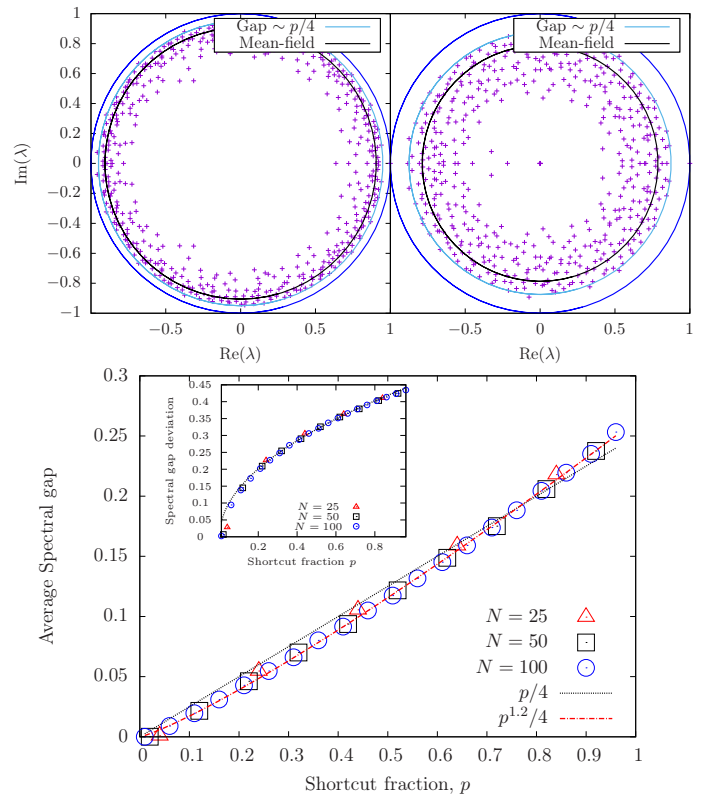


Figure 2: Top: Spectrum of the adjacency matrix of two SW networks, using  $N = 500$ , and  $p = 1/5$  (left) and  $1/2$  (right). Notice that most of the eigenvalues are contained within a ring, whose inner and outer radii are discussed in the text. Bottom: spectral gap for different values of  $N$  as a function of  $p$  of our SW networks, which grows approximately as  $p/4$ . A more accurate fit, with exponent 1.2 is also shown. Inset: Standard deviation of the gap scales as the square root of  $p$ .

A first requirement for complete synchronization is given by the GCD condition, which states that the number of possible synchronized subnetworks is equal to the Greatest Common Divisor (GCD) of the loop lengths of the network [12]. Hence, complete synchronization is only possible if the GCD of the lengths of all cycles in the network is unity. This is almost always the case for large enough networks with a finite number of shortcuts, as can be seen in Fig. 1 (bottom). When the GCD condition is met, the stability of the synchronization manifold is still determined by the eigengap as stated in Eq. (9).

The adjacency matrices  $G$  of directed networks are not hermitian, and their spectrum need not be real. Let us discuss the statistical properties of their spectra, in similarity to the studies of [27, 28]. Fig. 2 (top) shows the eigenvalues  $\{\gamma_i\}$  on the complex plane for two SW networks, using  $N = 500$  and  $p = 1/5$  (left) and  $1/2$  (right). Notice that, following Gerschgorin theorem, they are always contained within the unit circle. Except for the  $\gamma_1 = 1$  eigenvalue, which is a consequence of the row-sum condition, the phases of the eigenvalues seem to be homogeneously distributed. Moreover, they seem to be

contained within a ring, whose radius we would like to characterize.

An interesting approach to estimate the properties of the spectrum of random matrices describing SW networks was developed in [28], using a mean-field approach: write down the *average matrix*, whose entries are given by the average of the matrix entries. Due to translation invariance, the resulting matrix is a *circulant matrix*, whose spectrum can be found analytically. We have followed this approach in order to find the mean field spectrum of our SW networks. In the appendix A we show that the spectrum of this average matrix lies in the vicinity of a circumference of radius

$$|\gamma_m^{\text{MF}}| \approx \frac{1 - e^{-p}}{p}, \quad (10)$$

which appears marked in Fig. 2 (top) as *mean-field* line. Note that this mean-field theory does not provide an explanation for the ring structure of the spectrum. We have found numerically that the outer circumference has an approximate radius of  $(1 - p/4)$ , independent of  $N$ . Thus, our estimate for the gap is

$$\Delta \approx p/4, \quad (11)$$

The lower panel of Fig. 2 shows the numerical evidence for expression (11), plotting the average spectral gap as a function of  $p$  for different system sizes  $N$ . Interestingly, the inset shows that the deviation of the spectral gap among samples only grows like the square root of  $p$ ,  $\sigma_\Delta \sim p^{1/2}/2$ .

Once the spectral properties of our networks have been elucidated we can proceed to study their dynamics. We have simulated the dynamical system Eq. 1 and obtained numerically the synchronization Lyapunov exponent (SLE) for  $10^5$  different SW networks with  $N = 40$ ,  $T_d = 100$ ,  $\epsilon = 0.7$  and two values of  $p = 0.5$  and  $0.8$  and two maps: Bernoulli, Eq. (2), and Logistic, Eq. (3). We have chosen the numerical values of the parameters  $a = 1.1$  and  $r = 3.577$  so both maps have comparable Lyapunov exponents when considered in isolation, [33].

In Fig. 3 (top) we plot those values of the SLE vs the spectral gap of each network. In the Bernoulli case we find a nearly linear relationship, with a higher probability of synchronization (negative SLE) for  $p = 0.8$ . The Logistic case is more involved, but the negative correlation between both magnitudes is still clear. In general terms we can see that it synchronizes better.

Fig. 3 (bottom) shows the histogram of the SLE for Bernoulli and Logistic systems, using always  $N = 40$ ,  $T_d = 100$ ,  $\epsilon = 0.7$  and two values of  $p = 0.5$  and  $0.8$ . The black vertical bar marks the zero value: points on its left present stable synchronization. The histograms for the Bernoulli case have a nearly Gaussian shape, but with finite skewness and kurtosis [29]. The histograms are much more involved for the Logistic case.

We have also performed a thorough exploration of the parameter space,  $\epsilon$  and  $p$ , finding the average value of the SLE in Fig. 4 after 100 samples for each point, top for the Bernoulli map and bottom for the Logistic one. In both figures, red represents negative SLE, which allow for stable synchronization, while blue stands for positive values, which take away from synchronization. The white line in both represents the theoretical synchronization line, Eq. (9). It follows the zero SLE very accurately in the Bernoulli case, but not so in the Logistic one.

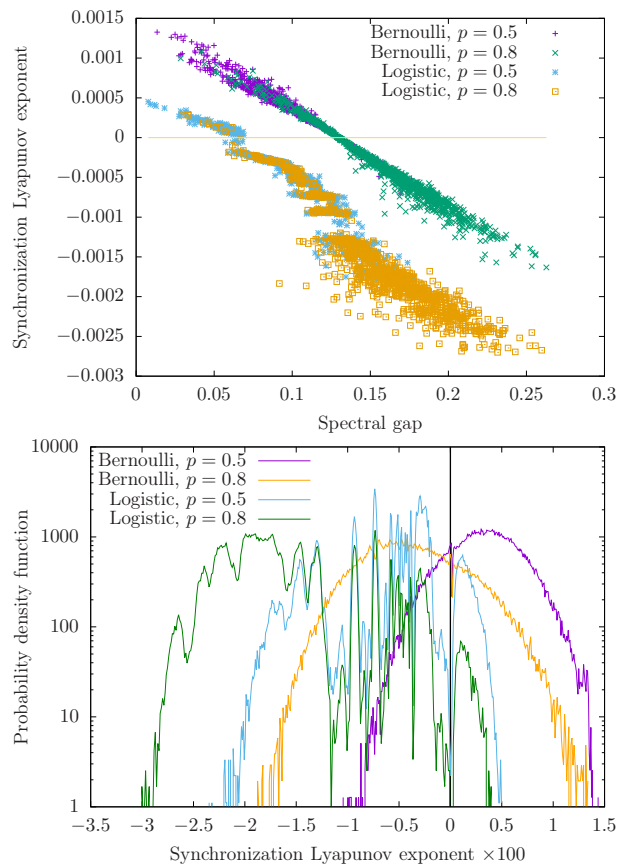


Figure 3: Measurement of the synchronization Lyapunov exponent (SLE) along with the spectral gap for two SW networks with  $N = 40$  sites,  $\epsilon = 0.7$ , and  $p = 0.5$  and  $p = 0.8$ , using two different dynamical systems: Bernoulli and Logistic, averaged over  $10^5$  samples. Top: Relation between the SLE and the spectral gap. Notice the nearly linear relation for the Bernoulli case. For the Logistic system, the correlation is still strong, but much more involved. Bottom: SLE histogram for the same four cases, in log-scale. Notice that, for Bernoulli we obtain an approximately Gaussian behavior, with non-zero skewness. For the Logistic case, the SLE are distributed in a much more complicated way. The vertical black bar marks the zero SLE, so on the left we have synchronization.



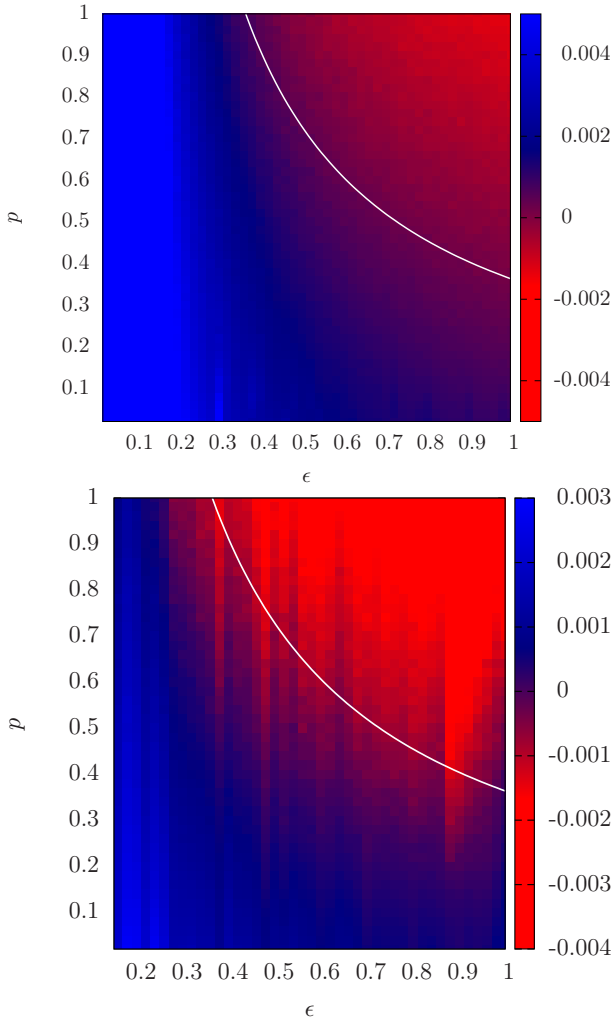


Figure 4: Average SLE for our SW networks as a function of both  $\epsilon$  and  $p$ , using 100 samples for each point. Top: Bernoulli map. Bottom: Logistic map. In white line, the theoretical prediction for the static synchronization line.

#### IV. FLUCTUATING NETWORKS

Let us allow our networks to fluctuate, making  $G$  time-dependent with a network switching period  $T_n$ . During the dynamics, the coupling topology will switch from the current network,  $G_{cur}$ , to a newly sampled  $G_{next}$  every  $T_n$  time steps. We will sample from the ensemble of all SW graphs with fixed  $N$  and  $p$  defined in section III. We will normalize each row by its sum so that the resulting networks verify the unit row-sum constraint (4) and the synchronized solution exists. The Bernoulli and Logistic map parameter values for  $a$  and  $r$ , respectively, will be the same as in the preceeding section III.

As a first attempt, we see in Fig. 5 a few histories for the synchronization of fluctuating SW networks of Bernoulli maps with  $N = 40$ ,  $p = 1/2$ ,  $\epsilon = 0.7$  and different fluctuation times:  $T_n = 10$ ,  $10^2$ ,  $10^3$  and  $10^4$ . Unless otherwise stated, we will always choose  $T_d = 100$

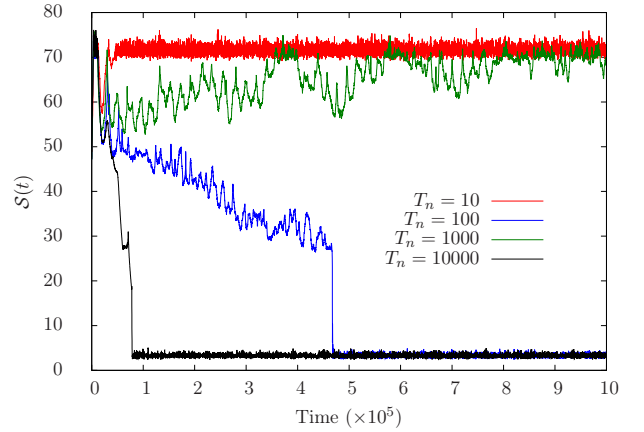


Figure 5: Synchronization level as a function of time for four histories of our dynamical system with  $N = 40$ ,  $p = 0.5$ ,  $T_d = 100$  and  $\epsilon = 0.7$  using different fluctuation times:  $T_n = 10$ ,  $10^2$ ,  $10^3$  and  $10^4$ . The units are Bernoulli maps.

for the time-delay. For  $T_n = 10^4$ , the synchronization level decays to its minimal value very fast, since the average SLE is positive, and full de-synchronization is irreversible. For  $T_n = 1000$ , we observe strong fluctuations in the state variance, but an ultimate synchronization. For  $T_n = 100$ , when the fluctuation time-scale coincides with the delay, the system also desynchronizes, although more slowly. For  $T_n = 10$ , the system synchronizes fully quite fast.

Let us average the synchronization level for a large enough number of histories (samples),  $N_s = 1000$ . Fig. 6 shows the results for three different systems of coupled Bernoulli maps, showing only time steps which are multiples of  $T_d = 100$ . In Fig. 6 (top) we show the average synchronization for the same system as Fig. 5, in order to assess whether those results are generic. We see that for very short fluctuation time  $T_n = 1$  or  $10$ , the system synchronizes quite fast. For  $T_n = 50$  the synchronization decays very slowly with time, and it decays much faster for  $T_n = 100$ . As we increase the fluctuation time scale, for  $T_n = 500$ , the synchronization decay is again a bit slower, and for  $T_n = 1000$  or  $2000$  we can see that the system does not seem to desynchronize, but stays at a lower level of synchronization than usual. For even slower fluctuations,  $T_n = 5000$ , the system desynchronizes again quite fast. We should also remark the presence of oscillatory behavior for short times.

The lower panels of Fig. 6 explore different systems. The central one shows the case of a Bernoulli system over SW networks with  $N = 40$ ,  $p = 0.8$  and  $\epsilon = 0.47$ , which is in average synchronizing. The main difference that we can observe is that for  $T_n = 100$  the system does not desynchronize, even though the asymptotic synchronization level is lower than for  $T_n = 50$  and  $T_n = 1000$ . For  $T_n = 10000$  the system still desynchronizes. One may ask how is it possible that, if the system is in average synchronizing, the system desynchronizes in the long run for slow network fluctuations. The reason is that,

for Bernoulli systems, desynchronization is *irreversible*. Once a certain threshold synchronization level is crossed, synchronizing networks will not take the system back. The short time oscillations that we observed in the previous case are still present, but attenuated.

The lowest panel of Fig. 6 shows the average synchronization level for a Logistic system on fluctuating SW networks with  $N = 40$ ,  $p = 1/2$  and  $\epsilon = 0.4$  (in average, non-synchronizing). Again, we observe that  $T_n = 100$ , coinciding with the time-delay, is specially bad for synchronization. In this case, there is a much stronger oscillation.

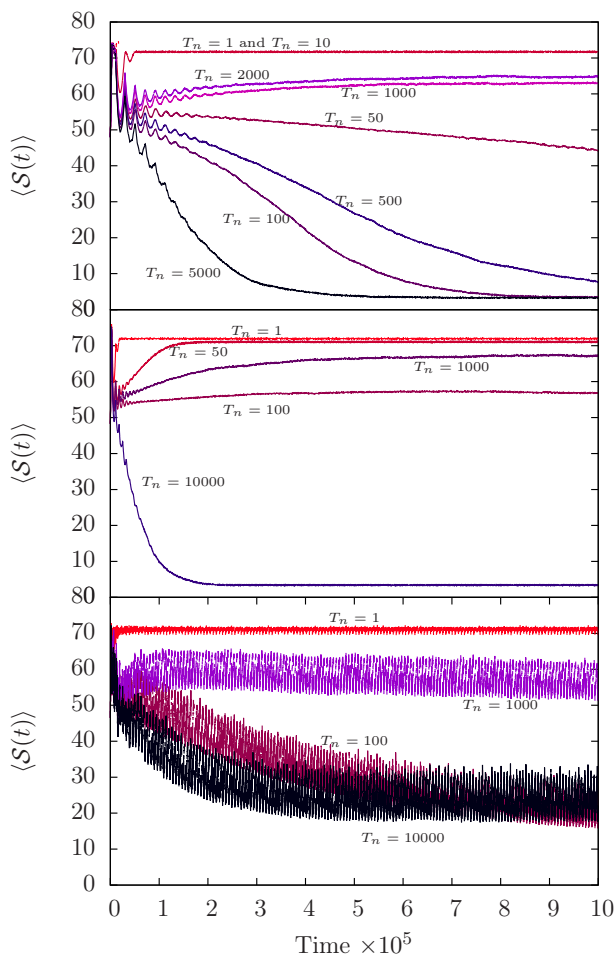


Figure 6: Realization average of the synchronization level,  $\langle S(t) \rangle$ , Eq. (7), over  $N_s = 1000$  samples, as a function of time for different systems. Top: Bernoulli system,  $N = 40$ ,  $p = 0.5$  and  $\epsilon = 0.7$  (in average, non-synchronizing), for different values of  $T_n$ . Center: Bernoulli system with  $N = 40$  sites,  $p = 0.8$  and  $\epsilon = 0.47$  (in average, synchronizing), for different values of  $T_n$ . Bottom: Logistic system,  $N = 40$ ,  $p = 0.5$  and  $\epsilon = 0.4$  (in average, non-synchronizing). In all cases,  $T_d = 100$ , and we only show time steps which are multiples of 100.

### A. Critical values of $\epsilon$

We have found out that, with all other parameters fixed, there is always a critical value of  $\epsilon$ , which we call  $\epsilon^*$  such that, if  $\epsilon > \epsilon^*$  the system stays synchronized almost surely, meaning that among the  $N_s = 1000$  samples launched, all of them stayed synchronized up to time  $10^6$ . Fig. 7 shows the critical  $\epsilon^*$  for Bernoulli systems as a function of the network fluctuation time, using fixed values for the other parameters,  $T_d = 100$  and  $p = 1/2$ . The three curves correspond to different system sizes  $N = 20$ , 40 and 80.

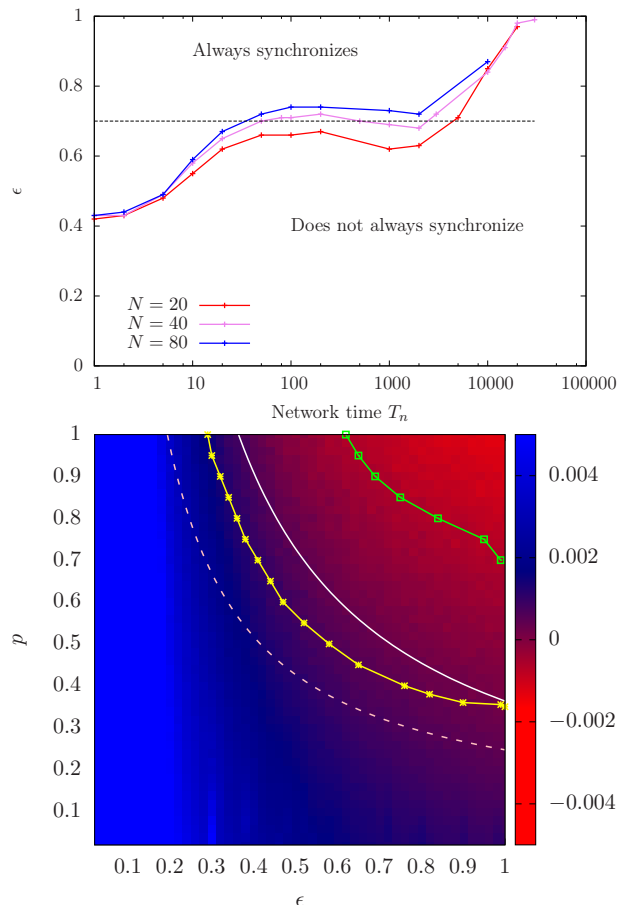


Figure 7: Top: Critical value  $\epsilon^*$  as a function of  $T_n$  for different values of  $N = 20, 40$  and  $80$ . In all cases,  $T_d = 100$  and  $p = 1/2$ , and the dynamical system is Bernoulli. The horizontal dashed line corresponds to the results shown in Fig. 6 (center),  $\epsilon = 0.7$ . Bottom: same SLE plot as a function of  $\epsilon$  and  $p$  as in Fig. 4, but adding extra lines. The yellow line denotes the  $\epsilon^*$  values as a function of  $p$  for very fast fluctuations,  $T_n = 10$ . Notice that even systems with positive average SLE will synchronize for those fast fluctuations. For comparison, the green line denotes the  $\epsilon^*$  value for very slow fluctuations,  $T_n = 10^4$ . The dashed pink line denotes the mean-field approximation given by Eq. (10). The continuous white line corresponds to the static network synchronization region and is included for comparison.

Notice that, for  $N = 40$  and  $\epsilon = 0.7$  the transition curve presents a reentrant behavior: the critical curve is crossed three times (see dashed horizontal line in Fig. 7). This explains the peculiar behavior found in the synchronization level averages in Fig. 6.

But Fig. 7 (top) provides more information. In all cases,  $\epsilon^*$  is minimal for small  $T_n$ . This implies that synchronization is most likely to happen for fast network fluctuations. Also, for very large  $T_n$  the values of  $\epsilon^*$  tend to one: synchronization in the long run becomes nearly impossible. For network fluctuation times  $T_n \sim T_d$  we have an interesting increase in the value of  $\epsilon^*$ , thus implying that when *both time-scales collide, synchronizability is lower*. This phenomenon bears similarity to observations reported on neural network models with spike-timing dependent plasticity [30].

The bottom panel of Fig. 7 shows the same average (static) SLE as a function of  $\epsilon$  and  $p$  for a Bernoulli system with  $N = 40$  and  $T_d = 100$ , marking also in white the zero SLE line, i.e.: synchronization in average. The yellow line marks the critical  $\epsilon^*$  line of almost-sure synchronization for  $T_n = 10$ , which is below the average synchronization line for static networks. This means that even values of the parameters which do not yield synchronization in average, will still synchronize almost surely when subject to fast fluctuations.

This enhancement of the synchronizability for rapidly fluctuating networks has also been observed in networks of oscillators with diffusive coupling [18, 21]. Moreover, the fast-switching approximation states that when the time-scale of the network fluctuations is much larger than the typical time-scale of the oscillator dynamics, the synchronization properties are well described by a mean-field network. This is not the case here: the pink dashed line in Fig. 7 (bottom) delimits the mean-field synchronization region expected from the spectrum in Eq. (10). As we can see, it departs from the yellow curve for fast network fluctuations, hence in our setting the mean-field curve does not provide a good approximation for the synchronization region of the fast switching regime, marked by the yellow curve. Notice that our setting is different from the classic fast switching approximation framework, which was developed for diffusive coupling. Instead, our couplings are given by the stochastic adjacency matrix and not by the Laplacian. Also, our internal time-scale  $T_d$  is a time-delay which does not inform us of the necessary time to reach synchronization, which could be in fact infinite for a non-synchronizing configuration. Still, the behaviour is qualitatively similar and the synchronizability is enhanced for  $T_n \ll T_d$ .

Finally, the green line shows the  $\epsilon^*$  line for  $T_n = 10^4$ . This corresponds to the static network regime  $T_n \gg T_d$ . The synchronization region is much smaller: for slow fluctuations, it is very difficult to force the system to synchronize.

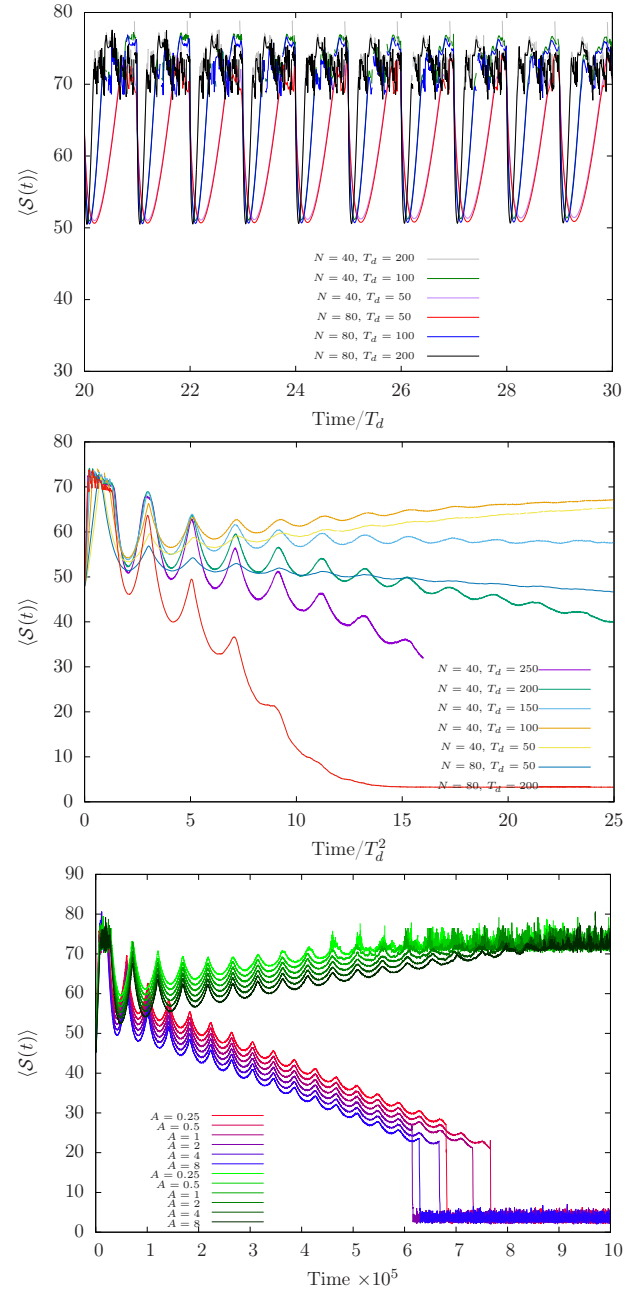


Figure 8: Top: Short-time evolution of the average synchronization level, with time in units of  $T_d$ , for  $p = 0.5$ ,  $\epsilon = 0.7$  and  $T_n = 1000$ , using different values of  $T_d$  and  $N$ . Center: Long time evolution, with the short period  $T_d$  filtered out and time in units of  $T_d^2$ . Notice that, in all cases, the oscillations have the same frequency and phase. Bottom: Average synchronization level for two fixed networks with  $N = 20$ ,  $p = 0.7$  and  $\epsilon = 0.83$ . The greenish sequence corresponds to a synchronizing instance, while the bluish sequence refers to a non-synchronizing one. In both cases, we have averaged over random initial perturbations with amplitude  $A \cdot 10^{-10}$ . Notice that, in all cases, we obtain oscillations with the same frequency and phase, but different amplitudes.

## B. Synchronization oscillations

A very salient feature of the average synchronization level curves in Fig. 6 is the presence of strong oscillations which decay with time. By inspection, we can see that they have the same frequency and phase for different values of  $T_n$ . Let us investigate those oscillations in more detail.

Fig. 8 (top) shows the average synchronization level for all time-steps (not only multiples of 100) using different values of  $N$  and  $T_d$ , for a short time-span, always with  $p = 1/2$ ,  $T_n = 1000$  and  $\epsilon = 0.7$ , with the time-axis rescaled to  $t/T_d$ . We can see that all the curves present the same frequency and phase. Thus, we claim the existence of a primary oscillation with period equal to the time-delay.

In Fig. 8 (center) we have removed this primary period, by showing only times multiple of  $T_d$ , and we represent a longer time span, with the time axis rescaled to  $t/T_d^2$ . In this case, again, the fluctuations have the same frequency and phase in all cases. Thus, we can conjecture that the average synchronization level presents a second period at  $T_d^2$ . Notice that the oscillation periods are unrelated to  $T_n$  and depend only on  $T_d$ .

In order to determine the origin of the oscillations, we have performed the following experiment, see Fig. 8 (bottom). We have selected two fixed networks with  $N = 20$ ,  $\epsilon = 0.83$  and  $p = 0.7$ . One of them synchronizes, and the other does not. Let us remind that the initial condition corresponds to a small random perturbation,  $\xi = A \cdot r$ , acting on a synchronized state. We have averaged over this initial condition, but using different amplitudes for the initial random perturbation following a geometric sequence: the amplitude is  $A \cdot 10^{-10}$  with  $A \in \{0.25, 0.5, 1, 2, 4, 8\}$ . We can see that in all cases the average synchronization presents an oscillation with the same frequency and phase, but increasing amplitude. Thus, we may conjecture that the origin of the oscillations is the memory of the initial perturbation.

## C. Low-gap networks

In order to explain the synchronization enhancement via network fluctuations we might conjecture that large gap networks pull the system towards the synchronization manifold, while low gap ones push it away. We have checked numerically that conjecture and found it to be inaccurate. In Fig. 9 we consider SW networks with  $N = 40$  and  $p = 1/2$ , on which we set up a Bernoulli interacting system with  $T_d = 100$  and  $\epsilon = 0.7$ . The difference is that the network fluctuations are only allowed to explore the ensemble of *low gap* graphs. Specifically, we reject all SW networks whose gap is larger than  $\Delta_* = 0.1$ . Approximately, the probability of rejection with these parameters is  $1/2$ . Nonetheless, the probability of one of these networks to synchronize is negligible ( $< 10^{-6}$  in our numerical experiments). Fig. 9 shows

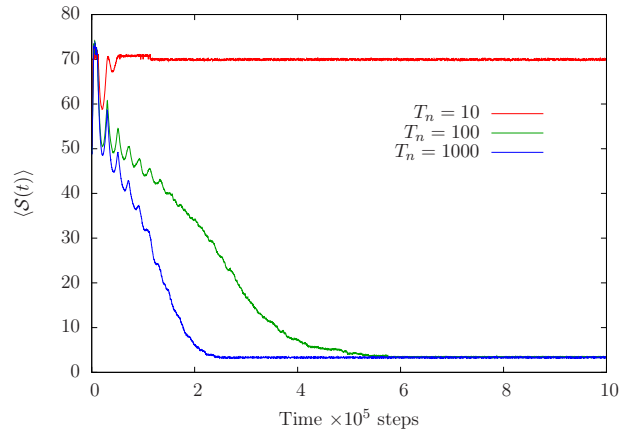


Figure 9: Average synchronization for Bernoulli systems with  $\epsilon = 0.7$  and  $T_d = 100$  on SW networks with  $N = 40$ ,  $p = 1/2$  and the additional constraint that the spectral gap will always be lower than  $1/10$ , value which is chosen because the probability for *each* network to synchronize under these conditions is negligible.

the average synchronization for 100 realizations, using  $T_n = 10, 100$  and  $1000$ , and found that, for fast enough fluctuations, the system *synchronizes*. Again, the same oscillations can be seen. This last result is reminiscent of the *Parrondo games* [31], where the alternation of losing strategies can give rise to a winning one. A random alternation of non-synchronizing networks can result strongly synchronizing.

## V. CONCLUSIONS AND FURTHER WORK

The possibility to enhance the stability of motion through fast oscillations or fluctuations is a topic of large tradition, e.g. the Kapitza pendulum [?]. In this work we have explored the effect of fluctuations on the synchronizability of time-delayed chaotic networks of small-world type with  $N$  nodes and a fraction  $p$  of shortcuts.

We have performed an analysis of the synchronizability of these networks when they are static, via a mean-field and a computational study of their spectral gap. The mean-field eigengap does not reproduce the experimental scaling which was found to be approximately given by  $p/4$ , independently of  $N$ . Thus, we may conjecture that this type of system is strongly influenced by network fluctuations. Nonetheless, for Bernoulli maps we find a very tight, relation between the synchronization Lyapunov exponent (SLE) and the spectral gap, which is more diffuse for Logistic systems.

The interplay between the time-scale of the delayed interactions,  $T_d$ , and that of the network fluctuations,  $T_n$ , give rise to very interesting situations. For the fast-switching regime,  $T_n \ll T_d$ , we obtain a strong enhancement of the synchronizability of the network. For  $T_n \sim T_d$  we observe a severe reduction in synchronizability, which is recovered as we increase  $T_n > T_d$ . Nonethe-



less, for  $T_n \gg T_d$  the system will nearly always desynchronize. Moreover, the average synchronization level is subject to strong oscillations, which are composed of several periods. We have identified at least two:  $T_d$  and  $T_d^2$ . They do not depend on  $T_n$ , and we provide evidence that they do not originate in the network fluctuations: the amplitude is shown to be proportional to the initial perturbation.

An intriguing feature of our results is that even when we restrict our network fluctuations to only explore those which would not be able to synchronize under static conditions, we can obtain almost-sure synchronization under fast enough fluctuations.

We have restricted ourselves to the case of small-world networks, because they are more amenable to a mean-field approach, but it is relevant to ask whether these results also apply to other network ensembles, such as purely random Erdős-Rényi graphs or scale-free networks. Also, other dynamical systems beyond Bernoulli or Logistic should be employed in order to clarify how generic our results are.

### Acknowledgments

We would like to acknowledge W. Kinzel, O. D'Huys and A. Deaño. This work was partly supported by the Spanish Government through grant FIS-2012-38866-C05-1 (J.R.-L.) and the Alexander von Humboldt Foundation within the Renewed research stay program (E.K.).

### Appendix A: Mean-field spectrum and eigengap of the SW networks

Our ensemble is composed of networks which consist of a directed ring of  $N$  nodes to which we add  $Np$  directed shortcuts. Here we compute the spectrum of the networks of this ensemble within the mean-field approximation of [28], in order to characterize the eigengap. The strategy is as follows: we obtain the ensemble average of each adjacency matrix entry,  $\langle G_{ij} \rangle$ , and study the spectrum of the resulting matrix, which will be a *circulant matrix*,

$$G^{\text{MF}} = \begin{bmatrix} c_0 & c_{N-1} & \dots & c_2 & c_1 \\ c_1 & c_0 & \dots & c_3 & c_2 \\ \vdots & \vdots & \ddots & \vdots & \vdots \\ c_{N-1} & c_{N-2} & \dots & c_1 & c_0 \end{bmatrix}, \quad (\text{A.1})$$

whose eigenvalues can be computed analytically [22]:

$$\gamma_m^{\text{MF}} = \sum_k c_k \exp \left[ \frac{-2\pi i m k}{N} \right], \quad (\text{A.2})$$

where  $m = 0, \dots, N-1$ . Before the shortcuts are introduced,  $c_1 = 1$  and all other entries  $c_i = 0$ ,  $i \neq 1$ . When

the shortcuts are introduced, the subdiagonal elements become  $G_{i,i+1} = 1/(1+n_s)$ , where  $n_s$  is the number of shortcuts reaching element  $i$ . Thus,

$$c_1 = \langle G_{i,i+1} \rangle = \left\langle \frac{1}{1+n_s} \right\rangle. \quad (\text{A.3})$$

The random variable  $n_s$  follows a binomial distribution: each site can be reached by  $\approx N$  possible shortcuts, each of them with probability  $\approx p/N$ . Thus, its probability distribution is given by

$$P(n_s) \approx \binom{N}{n_s} \left( \frac{p}{N} \right)^{n_s} \left( 1 - \frac{p}{N} \right)^{N-n_s}, \quad (\text{A.4})$$

which, in the limit where  $p/N \ll 1$  approaches the Poisson distribution

$$P(n_s) \approx e^{-p} \frac{p^{n_s}}{n_s!}. \quad (\text{A.5})$$

For this distribution it is possible to obtain the desired expected value:

$$\begin{aligned} c_1 &= \left\langle \frac{1}{1+n_s} \right\rangle \approx \sum_{n_s=0}^{\infty} \frac{1}{1+n_s} e^{-p} \frac{p^{n_s}}{n_s!} \\ &= \frac{e^{-p}}{p} \sum_{x=1}^{\infty} \frac{p^x}{x!} \\ &= \frac{1 - e^{-p}}{p}, \end{aligned} \quad (\text{A.6})$$

where we choose  $x = n_s + 1$ . The rest of the entries of the circulant matrix are all equal,  $c_i = \tilde{c}$  for  $i \neq 1$ , and can be found by normalization:

$$\tilde{c} \approx \frac{1}{N-1} \left( 1 - \frac{1 - e^{-p}}{p} \right), \quad (\text{A.7})$$

Thus, applying (A.2) we have

$$\gamma_m^{\text{MF}} = \tilde{c} + c_1 e^{\frac{2\pi i m}{N}} + \tilde{c} \sum_{k=2}^{N-1} e^{\frac{2\pi i k m}{N}}. \quad (\text{A.8})$$

If  $m = 0$ , we obtain  $\gamma_0 = 1$ . The last term can be evaluated as a geometric sum or, alternatively, we can realize that if  $k$  was extended from 0 to  $N-1$ , it would yield zero. In both cases, we obtain

$$\gamma_m^{\text{MF}} = (c_1 - \tilde{c}) e^{-\frac{2\pi i m}{N}}. \quad (\text{A.9})$$

Thus, the modulus of all eigenvalues for  $m > 0$  is equal:

$$|\gamma_m^{\text{MF}}| \approx c_1 - \tilde{c} = \frac{1 - e^{-p}}{p} - \frac{1}{N-1} \left( 1 - \frac{1 - e^{-p}}{p} \right). \quad (\text{A.10})$$

Neglecting corrections of order  $N^{-1}$ , we have our eigen-gap:

$$\Delta = 1 - \max \{ |\gamma_{m \neq 0}^{\text{MF}}| \} \approx 1 - \frac{1 - e^{-p}}{p}. \quad (\text{A.11})$$

- 
- [1] S. Boccaletti, J. Kurths, G. Osipov, D. Valladares, and C. Zhou, *Physics Reports* **366**, 1 (2002).
  - [2] L. M. Pecora and T. L. Carroll, *Phys. Rev. Lett.* **80**, 2109 (1998).
  - [3] V. Flunkert, S. Yanchuk, T. Dahms, and E. Schöll, *Phys. Rev. Lett.* **105**, 254101 (2010).
  - [4] F. M. Atay, J. Jost, and A. Wende, *Phys. Rev. Lett.* **92**, 144101 (2004).
  - [5] I. Fischer, R. Vicente, J. Buldu, M. Peil, C. Mirasso, M. Torrent, and J. Garcia-Ojalvo, *Phys. Rev. Lett.* **97**, 123902 (2006).
  - [6] M. Nixon, M. Fridman, E. Ronen, A. A. Friesem, N. Davidson, and I. Kanter, *Phys. Rev. Lett.* **108**, 214101 (2012).
  - [7] G. Buzsaki, *Rhythms of the brain* (Oxford University Press, 2006).
  - [8] I. Kanter, E. Kopelowitz, R. Vardi, M. Zigzag, W. Kinzel, M. Abeles, and D. Cohen, *EPL (Europhysics Letters)* **93**, 66001 (2011).
  - [9] A. Argyris, D. Syvridis, L. Larger, V. Annovazzi-Lodi, P. Colet, I. Fischer, J. García-Ojalvo, C. R. Mirasso, L. Pesquera, and K. A. Shore, *Nature* **438**, 343 (2005).
  - [10] I. Kanter, E. Kopelowitz, and W. Kinzel, *Phys. Rev. Lett.* **101**, 084102 (2008).
  - [11] T. Heil, I. Fischer, W. Elsässer, J. Mulet, and C. Mirasso, *Phys. Rev. Lett.* **86**, 795 (2001).
  - [12] I. Kanter, M. Zigzag, A. Englert, F. Geissler, and W. Kinzel, *EPL (Europhysics Letters)* **93**, 60003 (2011).
  - [13] M. J. Martin, O. D’Huys, L. Lauerbach, E. Korutcheva, and W. Kinzel, *Phys. Rev. E* **93**, 022206 (2016).
  - [14] J. Feng, V. K. Jirsa, and M. Ding, *Chaos* **16**, 015109 (2006).
  - [15] I. V. Belykh, V. N. Belykh, and M. Hasler, *Physica D: Nonlinear Phenomena* **195**, 188 (2004).
  - [16] F. Peruani, E. M. Nicola, and L. G. Morelli, *New Journal of Physics* **12**, 093029 (2010).
  - [17] N. Fujiwara, J. Kurths, and A. Díaz-Guilera, *Phys. Rev. E* **83**, 025101 (2011).
  - [18] M. Frasca, A. Buscarino, A. Rizzo, L. Fortuna, and S. Boccaletti, *Phys. Rev. Lett.* **100**, 044102 (2008).
  - [19] N. Fujiwara, J. Kurths, and A. Díaz-Guilera, *Chaos* **26**, 094824 (2016).
  - [20] M. Nag and S. Poria, *Chaos, Solitons & Fractals* **91**, 9 (2016).
  - [21] D. J. Stilwell, E. M. Bollt, and D. G. Roberson, *SIAM Journal on Applied Dynamical Systems* **5**, 140 (2006).
  - [22] G. H. Golub and C. F. Van Loan, *Matrix Computations* (Johns Hopkins University Press, 1996).
  - [23] S. Heilgental, T. Jüngling, O. D’Huys, D. A. Arroyo-Almanza, M. C. Soriano, I. Fischer, I. Kanter, and W. Kinzel, *Phys. Rev. E* **88**, 012902 (2013).
  - [24] M. Barahona and L. M. Pecora, *Phys. Rev. Lett.* **89**, 054101 (2002).
  - [25] M. Newman and D. Watts, *Physics Letters A* **263**, 341 (1999).
  - [26] D. J. Watts and S. H. Strogatz, *Nature* **393**, 409 (1998).
  - [27] R. Kühn, *Journal of Physics A: Mathematical and Theoretical* **41**, 295002 (2008).
  - [28] C. Grabow, S. Grosskinsky, J. Kurths, and M. Timme, *Phys. Rev. E* **91**, 052815 (2015).
  - [29] J. Billen, M. Wilson, A. Baljon, and A. Rabinovitch, *Phys. Rev. E* **80**, 046116 (2009).
  - [30] A. Knoblauch, F. Hauser, M.-O. Gewaltig, E. Körner, and G. Palm, *Frontiers in computational neuroscience* **6**, 55 (2012).
  - [31] G. P. Harmer and D. Abbott, *Nature* **402**, 864 (1999).
  - [32] S. N. Elaydi, *Discrete chaos: with applications in science and engineering* (CRC Press, 2007).
  - [33] The Lyapunov exponent of an isolated Bernoulli map is  $\lambda_B = \ln a \approx 0.09531$ . The Lyapunov exponent of the Logistic map,  $\lambda_L$ , must be obtained computationally, but a value of  $r = 3.577$  gives  $\lambda_B \approx \lambda_L$  [32].